Supplementary Information (SI) for Journal of Materials Chemistry A.
This journal is © The Royal Society of Chemistry 2026

SUPPLEMENTARY INFORMATION

Pulse-Mediated Refaceting of Copper. Influence on 5-Hydroxymethylfurfural Electrocatalysis

Vicente Pascual-Llorens,[a] Lorena Chico-Mesa,[b] Michael Musi,[c] Rosa M. Arán-Ais,*[b] Paula Sebastián Pascual*[a]

a. Wallenberg Initiative Materials Science for Sustainability, Department of Chemistry, School of Engineering Science in Chemistry, Biochemistry and Health, KTH Royal Institute of Technology, Stockholm, Sweden.

b. Instituto de Electroquímica, Universidad de Alicante, Apdo. 99, E-03080, Alicante, Spain.

c. SchoolUnit of Hultgren Laboratory for Materials Characterisation, Department of Materials Science and Engineering, KTH Royal Institute of Technology, Stockholm, Sweden.

*Corresponding author:

E-mail. rosa.aran@ua.es

E-mail: paulasp@kth.se

Additional SEM analysis of Cu(111) modified at different reduction potentials

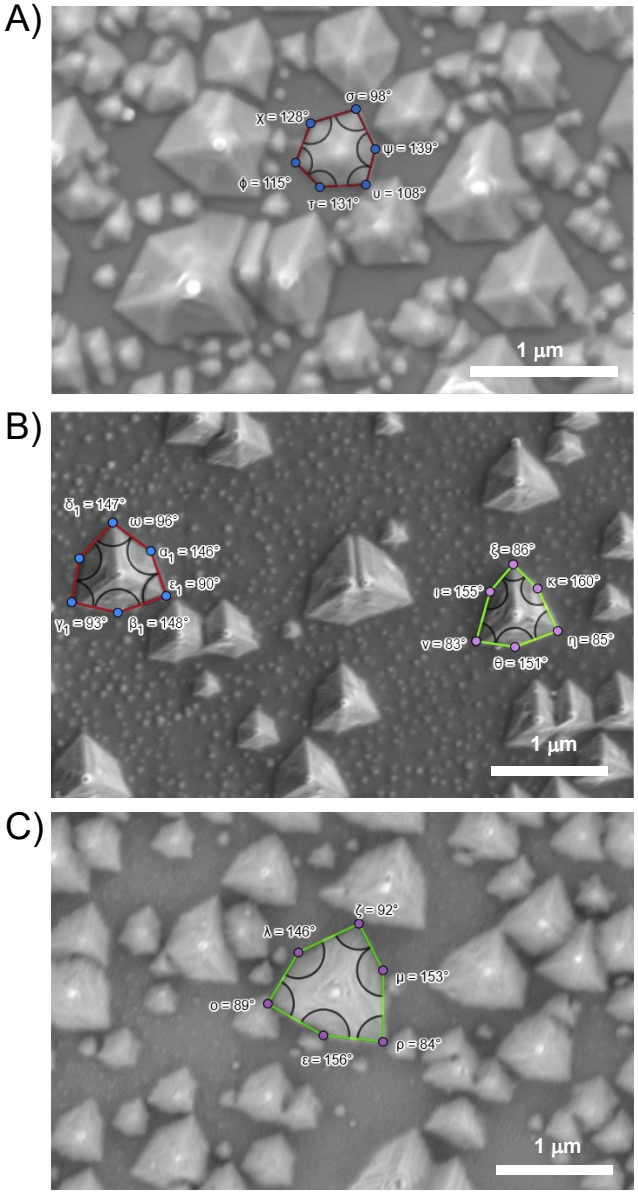

Figure S1. SEM images of the Cu(111) modified at three different E_R for 150 s: A) E_R = -1.30 V, B) E_R = -1.10 V and C) E_R = -0.90 V. We also show the angles for some of the deposited shaped morphologies.

Figure S1 displays SEM images of the shaped structures formed at three different reduction potentials. At -1.30 V (Figure S1A), the surface shows clusters with predominantly hexagonal shape, although some of them exhibit irregular, non-symmetrical sides. At -1.10 V (Figure S1B), the surface features a mixture of hexagonal shapes and others beginning to take on a triangular appearance. At -0.90 V (Figure S1C), most of the deposited structures appear regular

and less triangular than those observed at -1.00 V (Figure 1), suggesting that for potentials less negative than -1.00 V, the clusters gradually evolve back toward a hexagonal morphology.

For an equilateral hexagon, all the angles are 120°. Given that the Cu(S)[*n*(100)×(110)] surfaces correspond to the (*n*10) Miller indices, the transition from a hexagonal configuration ((*n*10) with a higher density of steps) to an equilateral triangular configuration ((*n*10) with extended (100) domains) involves the expansion of three angles to 180°, which define the lateral edges of the triangle, and the simultaneous contraction of the remaining three angles to 60°, which form its vertices. This evolution in shape and angles is represented in Figure S2. The more hexagonal feature in Figure S1A has two groups of angles. The first group of angles ranges from 128° to 140°, whereas the second group varies from 98° to 115°. In the more triangular features in Figure S1B and C, the difference between the two groups of angles is more pronounced, indicating the beginning of the transition from hexagonal to triangular shape. The first group of angles ranges from 150° to 158°, and the second group ranges from 83° to 90 °. This result indicates that the applied potential plays a crucial role in the formation of structures where the (100) domains expand. This hypothesis is later tested with CVs in NaCl used to decouple (100) terraces from steps in [*n*(100)×(h´k´l´)] geometries. The calculation involving angles was performed using GeoGebra software.

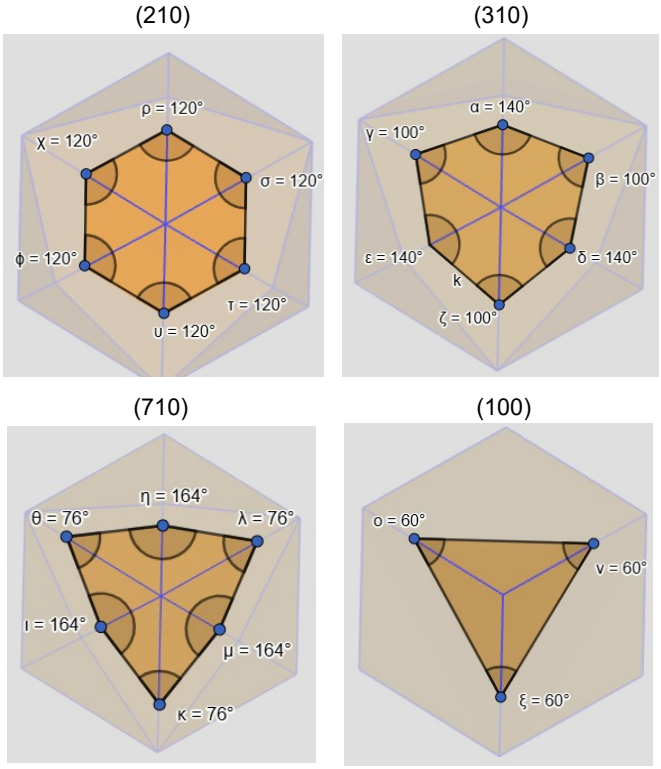

Figure S2. Simulation of the epitaxial growth of (*n*10) structures on a Cu(111) electrode and evolution of angles as *n* increases. The background shows a tetrahexahedral and cubic particle intersected by a (111) plane.

Determination of the electroactive surface area (ECSA) with Pb UPD

The formation of new sites was examined using the Pb UPD procedure. Different groups have used this methodology,[1–3] including us,[4] to make predictions on the facet distribution on copper surfaces. Figure S3 illustrates the SEM images and Pb UPD on a Cu(111) surface modified at E_R of -1.30 V, -1.00 V and -0.60 V, but for 300 s. The deposited morphological features (Figures S3A-E) are similar to those obtained at 150 s, but slightly bigger in size, leading to a more covered surface. The cathodic scan of the Pb UPD curves in Figure S3F shows several features related to Pb adsorption on different surface sites. The peak at -0.315 V (P1 in Figure S3A) is related to the (111) contribution, whereas the one at -0.355 V (P3 in Figure S3A) is linked to (*n*10) sites, as reported in our previous study.[3] The remaining broad feature, centred at -0.330 V (P2 in Figure S3A), was attributed to other geometries, likely defects or low-coordinated sites. Results in Figure S3A show that at E_R = -0.60 V, the surface is less modified, resulting in a less intense (*n*10) peak and a broader (111) peak. In contrast, the modifications at -1.30 V and -1.00 V provide similar Pb UPD profiles in which the (*n*10) features (P3) have similar intensity and shape. The main difference between them is that the (*n*10) feature (P3) at

-1.00 V is slightly broader and shifted to more negative potentials than at -1.30 V, i.e., is closer to the (100) region of the Pb UPD. This voltametric analysis shows that Pb UPD provides, to some extent, an overview of the site distribution on the surface. Still, this distinction is insufficient to differentiate high-index facet surfaces with varying step densities. This limitation likely arises from the fact that features corresponding to different facets and stepped contributions are distributed within a narrow potential window of lower than 100 mV in the Pb UPD curves. The significant overlap between peaks makes it nearly impossible to resolve all facet contributions using this method, highlighting the need for alternative electrochemical probes to identify terrace and step sites.

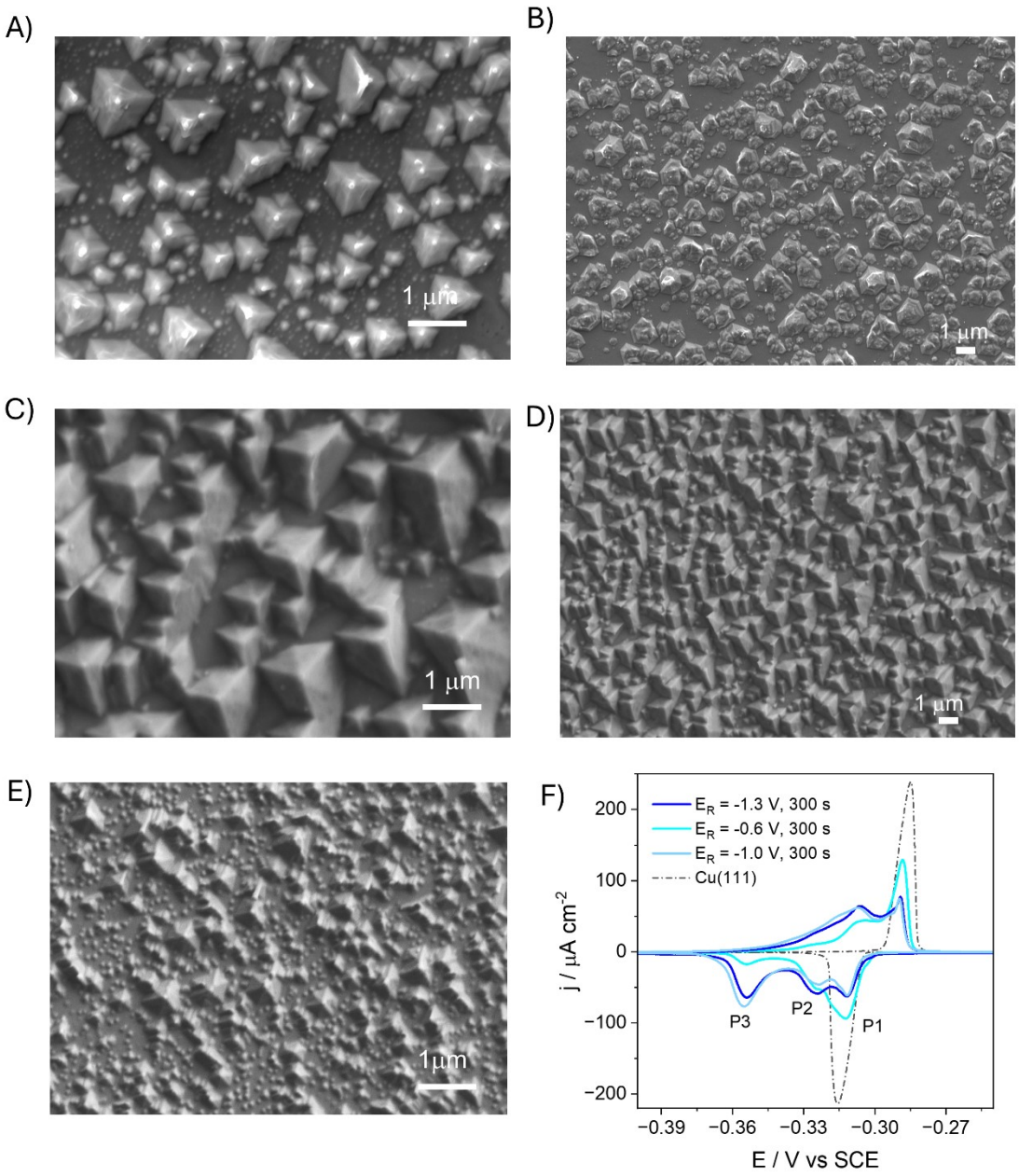

Figure S3. SEM of the Cu(111) electrode modified for 300 s at E_R of A) and B) -1.30 V, C) and D) -1.00 V and E) -0.60 V. F) Pb UPDs of modified Cu(111) at 5 mV s^{-1}.

To assess the change in electroactive surface area (ECSA) resulting from the pulse-mediated modification at different E_R, the roughness factor (RF) of each surface was determined following the next protocol. The charge of the cathodic scan in the Pb UPD curves was integrated, as this region exhibits more intense and well-defined peaks. Prior to integration, a baseline was created to subtract the capacitive current, which is minimal in Pb UPD CVs compared to the Pb adsorption/desorption peaks. The integrated charge (Q_{PbUPD} / $\mu C\ cm^{-2}$) was then normalised by the integrated charge of the unmodified Cu(111) and Cu(poly) substrates

($Q_{Cu(111)}$ / $\mu C\ cm^{-2}$ and $Q_{Cu(poly)}$ / $\mu C\ cm^{-2}$, respectively) to obtain the RF of each surface. For simplicity, variations in Pb UPD charge among different crystallographic single facets were not considered in the determination of the RF, as these are small according to our previous work.[3] The RF values determined for each Cu(111) and Cu(poly) modification are listed in Table S1.

	Cu(111)		**Cu(Poly)***	
E_R / V	Q / μC cm^{-2}	RF	Q / μC cm^{-2}	RF
Unmodified surface	386 ± 7	1	366	1
-0.60	399 ± 8	1.05 ± 0.02	410	1.12
-1.00	489 ± 8	1.27 ± 0.02	542	1.48
-1.30	481± 13	1.24 ± 0.03	505	1.38

Table S1. Summary of the calculated RF with Pb UPD for modified Cu(111) and for modified Cu(poly) at different E_R. The pulse duration was 300 s for Cu(111) refaceting and 180 s for Cu(poly) refaceting. (*) The integrated Q values and RF results for modified Cu(poly) were calculated using the voltammetric Pb UPD curves presented in Figure S6B.

The variations in RF with applied E_R are similar for both modified electrodes, with slightly higher RF values for Cu(poly).

Hard-sphere models for ideal turning point and stepped surfaces

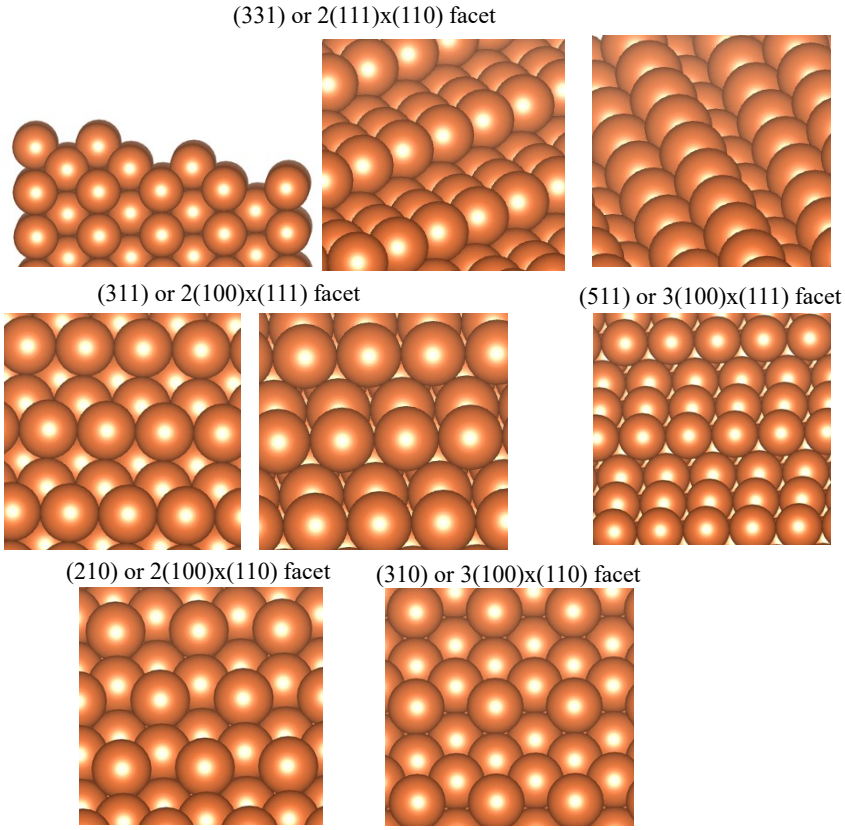

Figure S4. Atomic structures of (331), (210), and (311) turning points. The (311) and (210) show different perspectives of the same atomic arrangement. Atomic structures of (511) and (310) stepped surfaces (n=3) are also shown.

Determination of terrace and step contribution on pulse-modified Cu(111)

To estimate the proportion between (100) terrace domains and steps or defects on each refaceted Cu(111) electrode, charge integration of the anodic scans of the blank CVs in 0.1 M NaCl was performed. To decouple the charge contributions associated with (100) domains from those of steps and other defects, simulations of the experimental curves were first carried out using experimental reference voltammograms recorded on single-crystalline electrodes.

The positive-going scans were selected for analysis, as all single-crystal electrodes in Figure 2 exhibit sharp, well-defined peaks in the anodic curves. A baseline correction was applied to subtract the double-layer capacitance, isolating the faradaic charge contribution. Since the experimental datasets were acquired under slightly different potential scales, the

"Interpolate/extrapolate Y from X" function in Origin software was used to align the x-axis across all curves and build the simulated voltammograms.

Subsequently, the experimental voltammograms of the single facet surfaces were fitted to the experimental curves of the refaceted electrodes. To obtain the voltammetric profiles corresponding to the step contributions in (*n*10) and [n(100)x(111)] geometries, the defect-related features were extracted from the CVs of the (210), (310), and (311) surfaces. In the case of the (311) facet, which exhibits two distinct peaks, the curve was deconvoluted, and the lower-potential peak (designated as S1 in Figure 2) was isolated. The voltammogram of the Cu(110) single-crystal surface was used to represent the (110) defect contribution.

Figure S5 shows the comparison of the simulated curves and the ones obtained experimentally for the three E_R applied potentials (-1.30 V, -1.00 V, and -0.60 V). A strong correlation was observed in the low-potential region, where features associated with the (100) and (111) terraces are observed. However, the higher-potential region of the voltammogram, corresponding to step-related contributions, shows poorer agreement with the simulated curve. This discrepancy is tentatively ascribed to the inherently complex structure of the refaceted surfaces. The results suggest the presence of additional defect types contributing to the voltammetric response, likely concentrated at the apexes, edges, and other irregularities of the shaped deposits. The deviation between the simulated and experimental curves is most pronounced at -0.60 V, which corresponds to a defect-rich surface with fewer uniform clusters. In contrast, for the surface modified at -1.00 V, where the clusters are better defined, the difference between the simulated and experimental charges is approximately 5 $\mu C\ cm^{-2}$.

The close correspondence between the peak potentials in the experimental and single facet curves for step-related contributions is remarkable, indicating that NaCl still provides valuable information about which type of defect geometry and step is preferentially induced at each E_R. These results suggest that defects comprising (100) terrace sites adjacent to (111) or (110) steps are favoured when chloride acts as a coordinating ligand.

The good alignment of the curves in the low-potential region of the voltammogram further enables the distinction between terrace and defect contributions. This approach allows monitoring of the formation of (100) domains relative to steps and other low-coordinated sites as a function of the applied reduction potential during pulsing, while also providing an approximate estimate of the reduction of the (111) surface area by the newly formed structures.

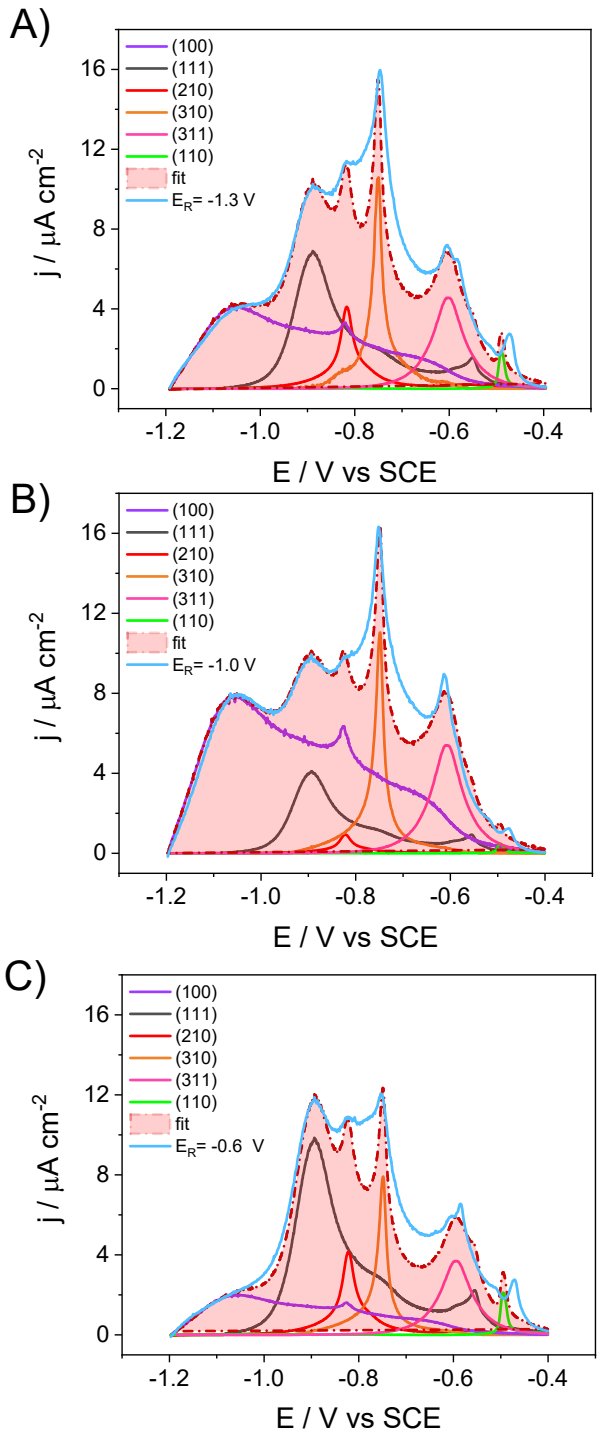

Figure S5. Anodic scans of the Cu(111) electrodes modified at three different E_R (blue line) recorded in 0.1 M NaCl at 50 mV s^{-1} and fitting of the curves (red area) using the voltammetric curves derived from model single facets. A) E_R = -1.30 V, B) E_R = -1.00 V, and C) E_R = -0.60 V. The fitting with the (310) and (311) facets only accounts for the step voltammetric feature, as the terrace feature is analogous to the feature of the (100) single crystal.

Table S2 summarises the integrated charges for (100) ($Q_{(100)}$) and (111) ($Q_{(111)}$) domains, and steps and other low coordinated sites (Q_{steps}) that are involved in the rest of the curves.

(1) $Q_{steps} = Q_{total} - Q_{(100)} - Q_{(111)}$

Reduction potential E_R / V	**Q / μC cm^{-2}**						
	Total	**(100) sites**	**(111) sites**	**Steps**	**%$Q_{(100)}$**	**% Q_{steps}**	**$Q_{(100)}$: Q_{steps}**
-0.60	84 ± 5	24 ± 6	29 ± 1	32 ± 5	28 ± 6	38 ± 6	**0.7**
-1.00	104 ± 3	60 ± 4	14± 2	30 ± 2	57 ± 3	29 ± 2	**2.0**
-1.30	101 ± 15	38 ± 9	23 ± 3	41 ± 2	37 ± 4	40 ± 4	**0.9**

Table S2. Integrated charges of the anodic region of the blank CVs in 0.1 M NaCl recorded for different modified Cu(111) surfaces. Table S2 also contains the integrated charges for the areas covered by the (100) and (111) terrace domains, which have been simulated using experimental curves from the (100) and (111) facets. The resulting integrated charge for steps and defects is obtained by subtracting the charge contribution of (111) and (100) domains from the total charge.

From the analysis of the blank cyclic voltammograms in NaCl electrolyte, as well as integrated charges for each facet contribution summarised in Table S2, some insights can be tentatively suggested:

(1) The modification at E_R of -1.00 V contains the highest amount of (100) terraces. Its charge contribution ($Q_{(100)}$) is higher than that of the modified surfaces at E_R of -1.30 V, and at E_R of -0.60 V. This result suggests that E_R of -1.00 V favours the formation of (100) terraces with increased length.

(2) Moreover, the integrated charge associated with step sites and defects is slightly higher at E_R of -1.30 V than at -1.00 V. This result indicates that higher deposition rates promote the development of defect-rich or step-dense domains over (100) terrace domains. These results are supported by SEM data, which clearly showed that at an E_R of -1.30 V, hexagonal morphologies resembling truncated tetrahexahedral clusters were formed.

(3) The integrated charge corresponding to (111) domains ($Q_{(111)}$) is the lowest at E_R = -1.00 V. Conversely, the surface modified at E_R = -0.60 V exhibits the highest $Q_{(111)}$ or

(111) terrace contribution, suggesting that too slow deposition rates cause minor surface refaceting.

(4) The integrated charge for steps and defects is similar for both E_R = -0.60 V and -1.00 V, even though at E_R = -0.60 V the substrate remains more exposed and less covered by new features. This observation suggests that when the deposition rate is too low, defects or steps form initially, but the limited growth kinetics prevent further faceting and the development of larger (100) terraces.

Electrochemical characterisation of the modified Cu(poly)

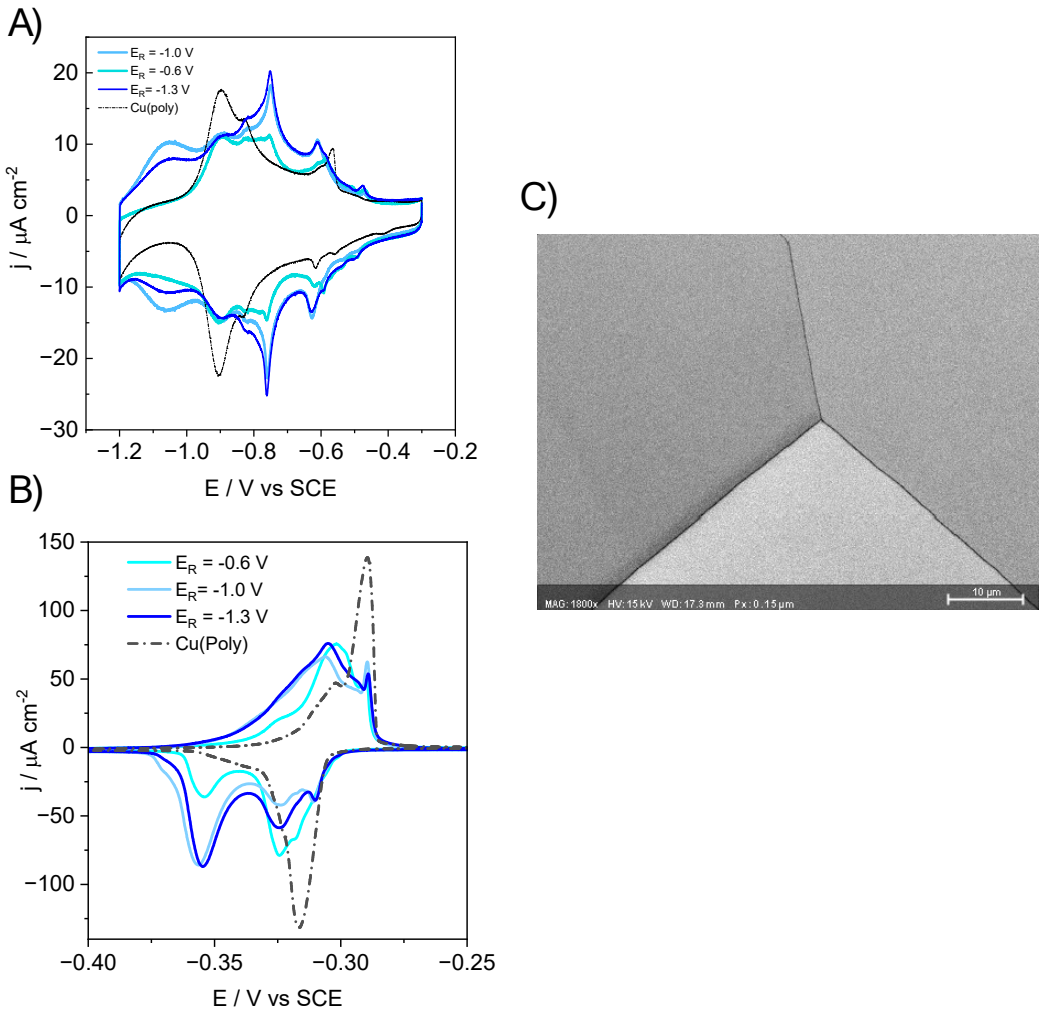

Figure S6. A) Blank CVs of the Cu(poly) modified at different E_R in 0.1 M NaCl at 50 mV s^{-1} B) Pb UPD CVs of the same modified Cu(poly) surfaces at 5 mV s^{-1}. C) SEM image of the pristine electropolished Cu(poly), showing well-defined grain boundaries.

Figure S6 compares the blank CVs in NaCl with the Pb UPD CVs for the Cu(poly) electrodes modified at -1.30 V, -1.00 V and -0.60 V for 180 s. Figure S6A shows the results in NaCl, which are similar to those obtained on Cu(111) modified at different E_R. Figure S6B shows the corresponding Pb UPD CVs. At -1.00 V, the CV displays a broader peak centred at -0.355 V, associated with (*n*10) domains, and a small shoulder at -0.367 V that is absent at E_R = -1.30 V, supporting the formation of larger (100) domains at E_R = -1.00 V. The RFs of modified Cu(poly) electrodes at distinct E_R are summarised in Table S1. Figure S6C shows a SEM image of the pristine Cu(poly), showing the grain boundaries.

Electrochemical characterisations in NaOH and geometric activities for the HMF electrocatalysis

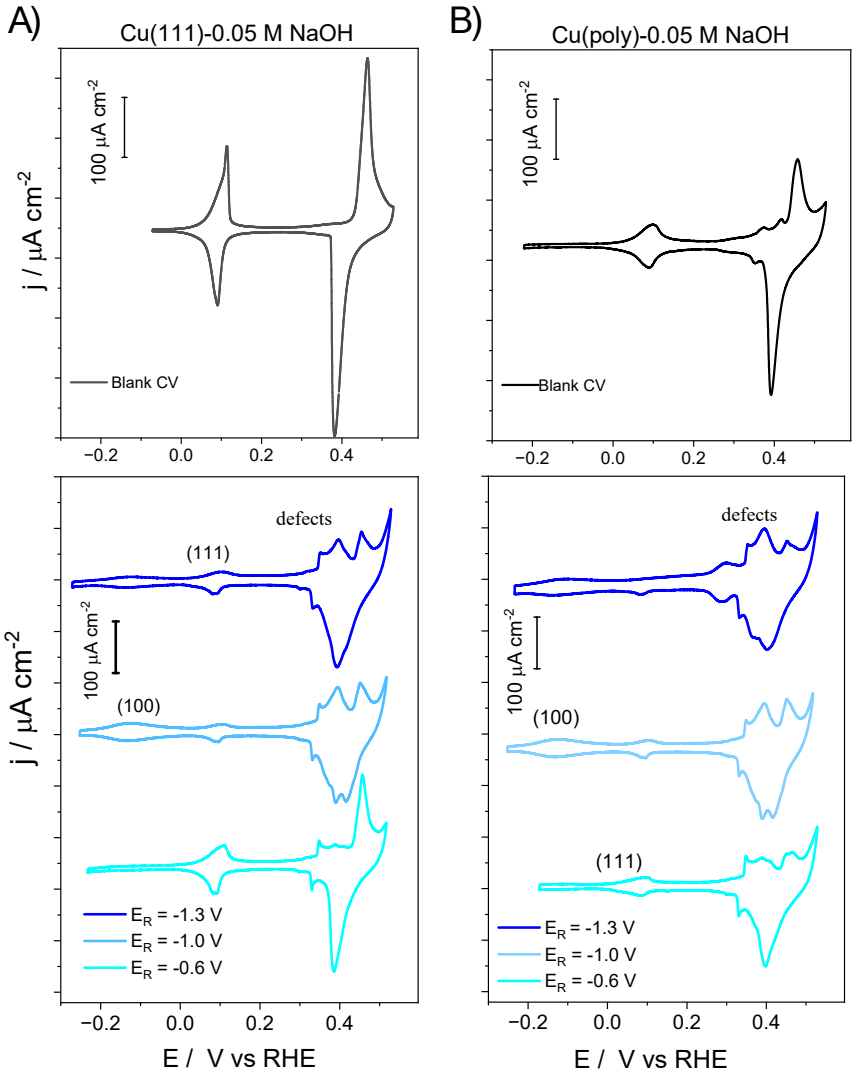

Figure S7. Blank CVs of pristine and modified copper surfaces at different E_R, in 0.05 M NaOH at 50 mV s^{-1}. A) Cu(111) and B) Cu(poly).

The CVs in NaOH electrolyte clearly separate the (100) and (111) terrace sites but cannot easily distinguish between defects with different geometries due to the overlap in the upper region of the voltammetric profiles, which also appear close to the Cu(111) pre-oxide formation peak. The blank CV of Cu(111) in A) was recorded at a markedly shorter cathodic limit to avoid the potential region where the electrode reconstructs, thereby distorting the sharp feature at -0.10 V vs RHE, as reported in previous work.[5]

Figure S8 depicts the geometric activities of the HMF oxidation and reduction CVs on different refaceted Cu(111) and Cu(poly) electrodes.

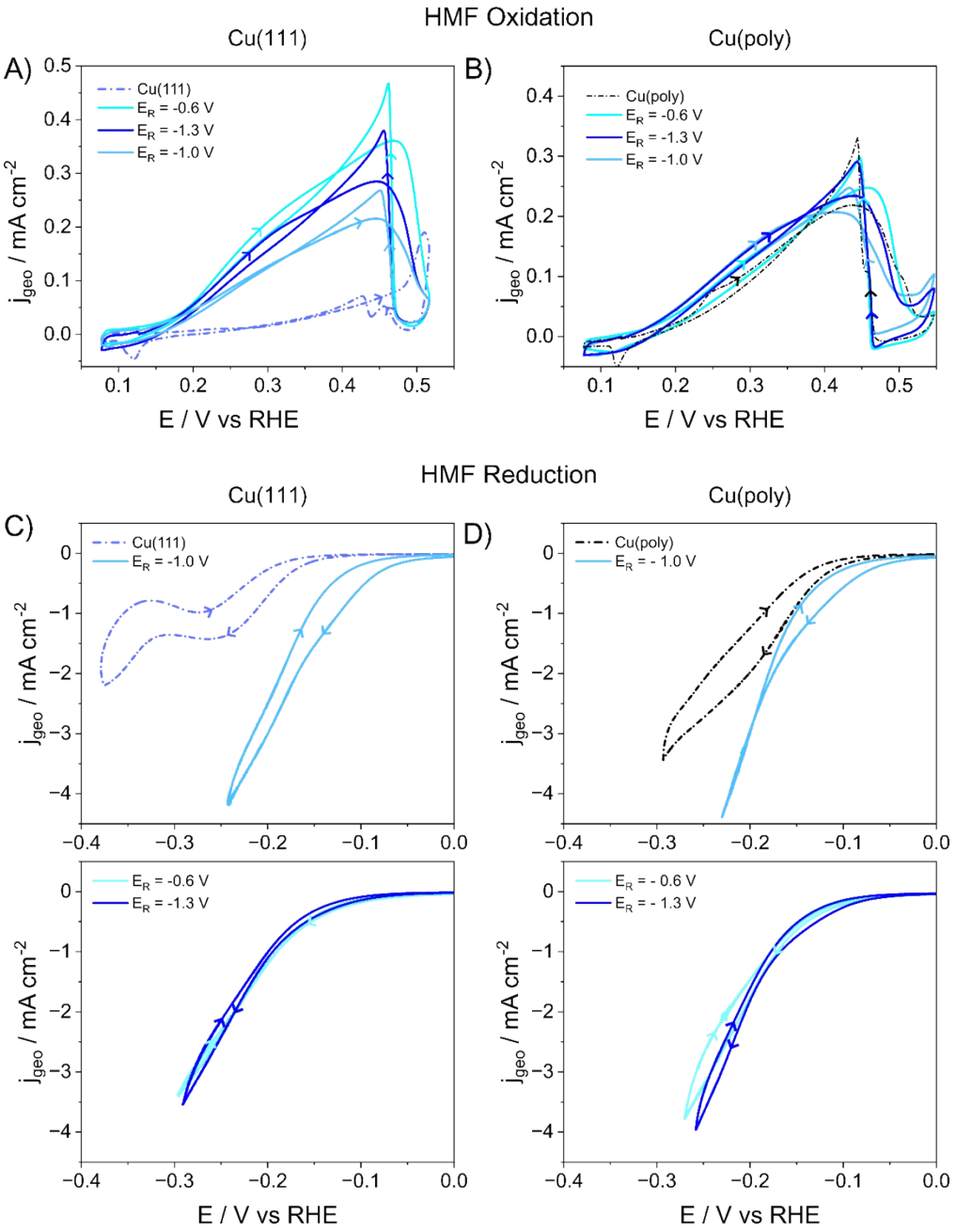

Figure S8. CVs of the HMF oxidation and reduction in 50 mM HMF and 0.05 M NaOH solution at 10 mV s^{-1}. HMF oxidation on modified A) Cu(111) and B) Cu(poly) at different E_R; CVs (first cycle) of the HMF reduction on modified C) Cu(111) and D) Cu(poly) at the same applied E_R. The HMF reduction in C) and D) are manually IR corrected (100% correction), whereas the HMF oxidation in A) and B) are not IR corrected to avoid distorting the voltametric sharp peak.

Stability of different refaceted and single crystal copper surfaces

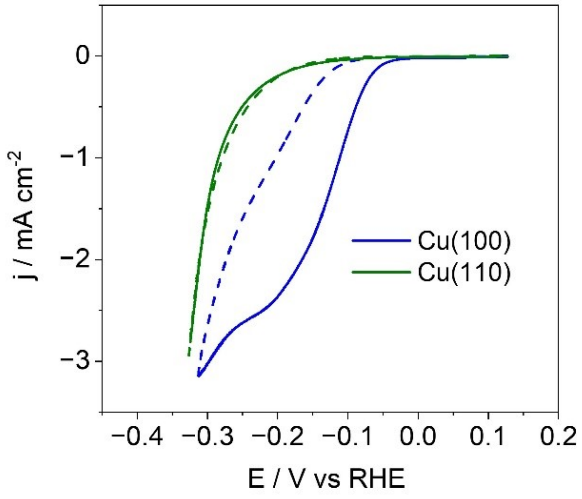

Figure S9. CVs of HMF reduction on Cu(100) and Cu(110) in 50 mM HMF and 0.05 M NaOH at 10 mV s^{-1}. The solid line represents the cathodic or reduction CV scan, whereas the dashed line represents the reversed or anodic scan.

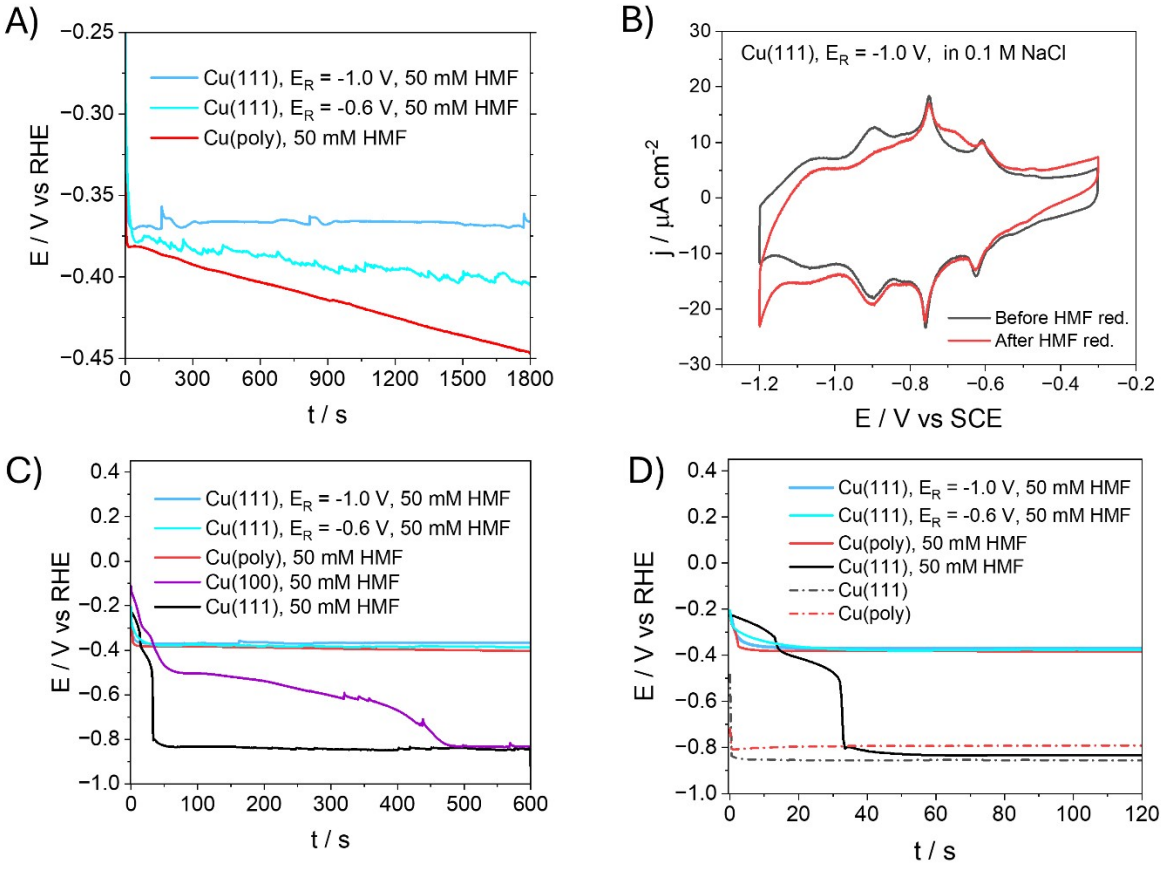

Figure S10. Stability tests. Chronopotentiometry transients recorded at constant current density of -2.5 mA cm^{-2} for 30 minutes on A) Cu(poly), Cu(111) modified at E_R of -1.00 V and -0.60 V, in 50 mM HMF. B) Shows the blank CV of Cu(111) refaceted at E_R = -1.00 V before

and after HMF electrolysis. C) Includes the chronopotentiometry transients of Cu(111) and Cu(100) to illustrate the fast deactivation of single crystals compared to refaceted surfaces at moderate conversion rates. D) Includes the chronopotentiometries of Cu(poly) and Cu(111) in the absence of HMF to illustrate HER potential. The electrode potential plotted in y-axis of Figures S10 A, C and D, has been IR corrected. Ohmic drop varies between 390 and 400 Ohm. The applied current density (-2.5 mA cm^{-2}) is calculated using the estimated ECSA in refaceted copper, as the rougher refaceted surface has a slightly higher density of active sites per unit of electrode area than flat Cu(poly), Cu(111), and Cu(100).

Software used in this work

VESTA 3 for three-dimensional visualization of crystal for the modelling of the epitaxial growth of shaped particles on copper.[6] *GeoGebra* was used for the calculation of angles in shaped structures.[7]

References

1 C. Zhan, F. Dattila, C. Rettenmaier, A. Herzog, M. Herran, T. Wagner, F. Scholten, A. Bergmann, N. López and B. Roldan Cuenya, *Nat. Energy*, 2024, **9**, 1485–1496.

2 D. Hochfilzer, A. Tiwari, E. L. Clark, A. S. Bjørnlund, T. Maagaard, S. Horch, B. Seger, I. Chorkendorff and J. Kibsgaard, *Langmuir*, 2022, **38**, 1514–1521.

3 P. M. Couce, T. K. Madsen, E. Plaza-Mayoral, H. H. Kristoffersen, I. Chorkendorff, K. N. Dalby, W. van der Stam, J. Rossmeisl, M. Escudero-Escribano and P. Sebastián-Pascual, *Chem. Sci.*, 2024, **15**, 1714–1725.

4 V. Pascual-Llorens, A. Serrà-Ramos and P. Sebastián-Pascual, *Electrochim. Acta*, 2025, **518**, 145793.

5 P. Sebastian-Pascual, F. J. Sarabia, V. Climent, J. M. Feliu and M. Escudero-Escribano, *J. Phys. Chem. C*, 2020, **124**, 23253–23259.

6. Momma, K.; Izumi, F. VESTA 3 for three-dimensional visualization of crystal, volumetric and morphology data. J. Appl. Crystallogr., 2011, 44, 1272–1276. https://doi.org/10.1107/S0021889811038970

7. Hohenwarter, M.; Preiner, J.; Yi, T.; Lavicza, Z. *GeoGebra 5.* ZDM – Mathematics Education, 2018, 50, 1085–1098. https://doi.org/10.1007/s11858-018-0994-6